ChemComm

Accepted Manuscript

This article can be cited before page numbers have been issued, to do this please use: H. Ogasawara, M. Grzybowski, R. Hosokawa, Y. Sato, M. Taki and S. Yamaguchi, *Chem. Commun.*, 2017, DOI: 10.1039/C7CC07344E.

ROYAL SOCIETY OF CHEMISTRY

rsc.li/chemcomm

View Article Online
DOI: 10.1039/C7CC07344E

Chemical Communications

COMMUNICATION

A far-red fluorescent probe based on a phospha-fluorescein scaffold for cytosolic calcium imaging

Received 00th January 20xx,
Accepted 00th January 20xx

DOI: 10.1039/x0xx00000x

www.rsc.org/

Hiroaki Ogasawara,[a] Marek Grzybowski,[b] Riho Hosokawa,[a] Yoshikatsu Sato,[b] Masayasu Taki,*[b,c] Shigehiro Yamaguchi*[a,b]

The far-red emissive fluorescent probe CaPF-1 based on a phospha-fluorescein scaffold enables the detection of cytosolic calcium ions in living cells. The probe can be excited in the red region (λ_{abs} = 636 nm) and exhibits a sufficiently high fluorescence turn-on response in the far-red region (λ_{em} = 663 nm) upon complexation with calcium ions. The hydrophilic and anionic characteristics of this phospha-fluorescein fluorophore allowed the cytosolic localization of CaPF-1. Moreover, it was possible to visualize histamine-induced calcium oscillation in HeLa cells using CaPF-1.

Calcium (Ca^{2+}) probes enable the visualization of neuronal Ca^{2+} dynamics related to synaptic activity in single cells and in the entire brain.[1–3] In the past three decades, various types of fluorescent probes for imaging intracellular Ca^{2+} ions have been developed, including small-molecule[4–6] and fluorescent protein-based (e.g. cameleon and GCaMP) probes,[7–9] as well as a hybrid system between genetically encoded proteins and molecular probes (e.g. SNAP-tag and O^6-benzylguanine-conjugated molecular probes).[10] In combination with recently developed microscopic imaging techniques, Ca^{2+} transients in neuronal networks have been successfully monitored *in vivo* with high spatiotemporal resolution.[1–3]

For the elucidation of the details of intracellular Ca^{2+} signaling, probes furnishing absorption and emission in the far-red to NIR region (λ = 650-900 nm) are preferred, as these probes can minimize background signals arising from autofluorescence, scattering of excitation and emission light, and the effect of laser stimulation on biological activities.[11,12] From this point of view, several fluorescent Ca^{2+} probes performing in this wavelength region have been developed using squaraine,[13] cyanine,[14] hemicyanine,[15] silicon-rhodamine,[16] and BODIPY[17] as the fluorophore scaffold. Some of these probes were successfully employed for monitoring Ca^{2+} dynamics in living cells[17] or in brain slices[16] under the excitation with common red lasers (He-Ne laser: 633 nm; laser diode: 635 nm).

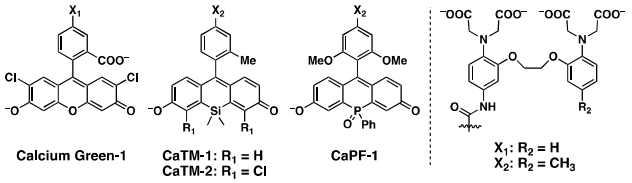

Fig. 1 Chemical structures of the Ca^{2+} probes Calcium Green-1, CaTM-X (X = 1, 2), and CaPF-1, which are based on fluorescein, sila-fluorescein (TokyoMagenta), and phospha-fluorescein (PF) scaffolds, respectively.

Table 1 Photophysical Properties of Fluorescent Ca^{2+} Probes Based on a Fluorescein-analogue.

Ca^{2+} probes	λ_{abs} / nm	λ_{em} / nm	Φ_F (Ca^{2+}-free)	Φ_F (Ca^{2+}-bound)	fluorescence turn-on ratio
CaPF-1	636	663	~0.02	0.22	13
Calcium Green-1	506	531	0.13	0.75	6
Fluo-3	508	527	<0.005	0.14	>100
CaTM-1	585	603	0.066	0.37	5.6
CaTM-2	597	609	0.024	0.39	16

However, the cytosolic diffusibility and membrane permeability of these probes still remain to be improved. Fluorescein and its derivatives represent promising fluorophores to this end, as their inherent negative charge allows passive diffusion into the cytosol. Hanaoka and co-workers have developed the red-emissive Ca^{2+} probes CaTM-X (X = 1, 2) based on a TokyoMagenta (TM) fluorophore,[18] wherein an endocyclic oxygen atom of the fluorescein is replaced with a silicon atom (Fig. 1). As observed with the fluorescein-based Ca^{2+} probe Calcium Green-1 (Fig. 1),[19] these red-fluorescent probes allow the monitoring of cytosolic Ca^{2+} ions. For the long-term fluorescence imaging of Ca^{2+} in live samples under the cell-friendly conditions, the use of

[a] Department of Chemistry, Graduate School of Science and Integrated Research Consortium on Chemical Sciences (IRCCS), Nagoya University, Furo, Chikusa, Nagoya 464-8602, Japan.
[b] Institute of Transformative Bio-Molecules (WPI-ITbM), Nagoya University, Furo, Chikusa, Nagoya 464-8601, Japan. E-mail: taki@itbm.nagoya-u.ac.jp, yamaguchi@chem.nagoya-u.ac.jp
[c] JST-PRESTO, 4-1-8, Honcho, Kawaguchi, Saitama 332-0012, Japan.

† Electronic Supplementary Information (ESI) available: Synthetic details, photophysical and electrochemical data, and cell culture experiments. See DOI: 10.1039/x0xx00000x

View Article Online
DOI: 10.1039/C7CC07344E

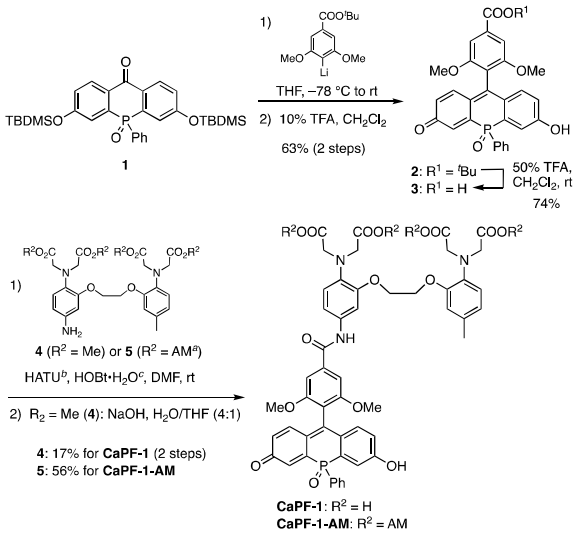

Scheme 1. Synthesis of CaPF-1 and its acetoxymethyl ester CaPF-1-AM; [a]AM: acetoxymethyl [b]HATU: 1-[bis(dimethylamino)methylene]-1H-1,2,3-triazolo[4,5-b]pyridinium 3-oxid hexafluoro-phosphate; [c]HOBt·H2O: 1,2,3-benzotriazol-1-ol monohydrate.

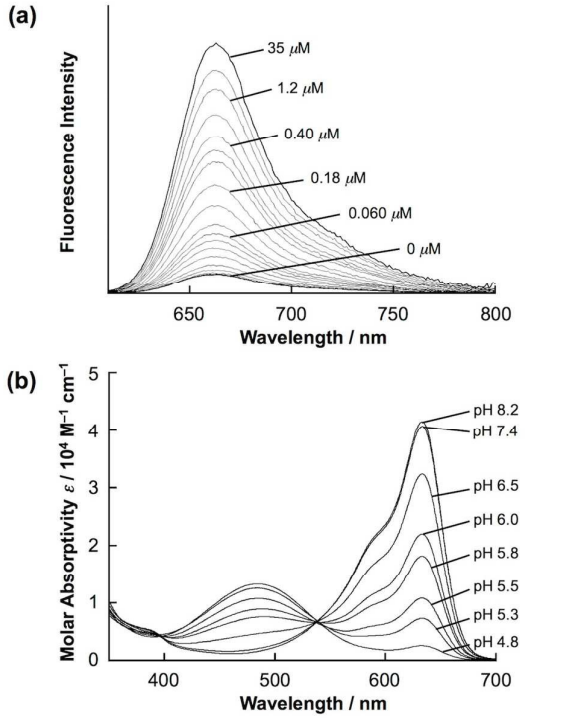

Fig. 2 (a) Emission spectra of CaPF-1 (1 μM) observed under excitation (λ_{ex} = 580 nm) in 50 mM HEPES (pH = 7.4), containing various concentrations of Ca^{2+} ions. (b) Absorption spectra of CaPF-1 (10 μM) as a function of the pH value.

fluorescence probes with longer excitation and emission wavelengths as well as higher photostability are more desirable.[16]

In this context, we have recently developed the far-red emitting fluorescein analogue phospha-fluorescein (PF), which contains a phosphine oxide (P=O) moiety at the 10-position of the fluorescein.[20–22] Due to its low-lying LUMO, which results from the electron-withdrawing effect of the phosphine oxide moiety, and its narrow HOMO–LUMO gap, which arises from the effective σ^*–π^* conjugation, PF exhibits its longest absorption maximum at λ_{abs} = 627 nm, and its emission maximum at λ_{em} = 656 nm in neutral aqueous buffer. Moreover, PF exhibits excellent photostability and a low pK_a value of 5.7 for the phenolic OH group in the xanthene skeleton.[20–22] These characteristics should be advantageous for the development of far-red-emitting fluorescence probes for Ca^{2+} ions. Herein, we report the design and synthesis of the far-red-emitting Ca^{2+} probe CaPF-1 based on a phospha-fluorescein scaffold (Fig. 1). We anticipated that the anionic nature of CaPF-1 at pH = 7 should facilitate its cytosolic localization. Moreover, the practical utility of CaPF-1 for Ca^{2+} imaging, particularly in living cells, was evaluated in this study.

CaPF-1 contains a 1,2-bis(*o*-aminophenoxy)ethane *N,N,N′,N′*-tetraacetic acid (BAPTA) moiety, which acts as a Ca^{2+}-specific binding site and as an electron donor in the photo-induced electron transfer (PET) system.[18,19] We employed a 2,6-dimethoxy phenyl group as a linker between the BAPTA ligand and the PF fluorophore in order to improve the chemical stability against nucleophilic attacks at the 9-position of the xanthene skeleton.[22,23] The synthesis of CaPF-1 is outlined in Scheme 1. Phospha-xanthone precursor **1** was treated with *in-situ*-generated 4-*tert*-butoxycarbonyl-2,6-dimethoxyphenyllithium, which furnished PF fluorophore **2** in 63% yield. A subsequent deprotection of the *tert*-butyl ester afforded 4-carboxy PF **3** in 74% yield. A condensation reaction between **3** and the methyl ester of the BAPTA ligand **4**, followed by hydrolysis, afforded CaPF-1 in 17% yield. It is worth noting that **3** should be useful as a common precursor for various far-red emitting PET-based probes.

The photophysical properties of CaPF-1 and its Ca^{2+}-bound form (1 μM) were investigated in HEPES buffer solutions (50 mM, pH = 7.4) in the absence and presence of 1 mM Ca^{2+} ions, respectively (Fig. S1, ESI†). As CaPF-1 is based on the PET mechanism, both species showed identical absorption bands (λ_{abs} = 636 nm, ε = 41500 M^{-1} cm^{-1}). In contrast, a ~13-fold increase of the fluorescence intensity at 663 nm was observed upon complexation with Ca^{2+} (Ca^{2+}-free: Φ_F ~0.02; Ca^{2+}-bound: Φ_F = 0.22). The fluorescence turn-on ratio (TOR) observed for CaPF-1 (TOR = 13) is larger than that for CaTM-1 (TOR = 5.6) and comparable to that for CaTM-2 (TOR = 16).

The driving force of the PET process can be estimated by the Rehm-Weller equation, which combines the oxidation potential (E_{ox}) of the PET donor, the reduction potential (E_{red}) of the fluorophore, the 0-0 transition energy (ΔE_{00}), and electrostatic correction term. Because CaPF-1 and Calcium Green-1 contain the common PET donor, E_{ox} values of these probes should be identical, meaning that the PET efficiency in water can be considered by comparing the E_{red} and ΔE_{00} values of the fluorophores. The ΔE_{00} value of CaPF-1 (1.91 eV) is much smaller than that of fluorescein-based Calcium Green-1 (2.39 eV), indicative of an unfavorable Gibbs energy for the PET quenching process, which is inevitable for far-red dyes.

View Article Online
DOI: 10.1039/C7CC07344E

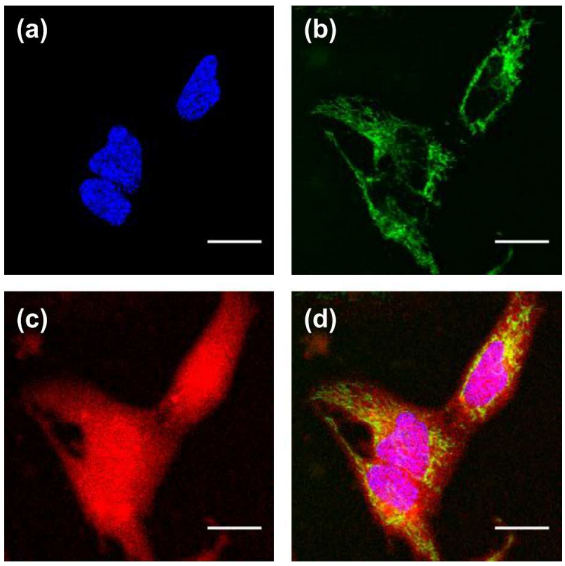

Fig. 3 Three color imaging of (a) nucleus, (b) mitochondria, (c) cytosolic Ca^{2+} in HeLa cells stained with Hoechst 33342 (λ_{ex} = 405 nm; λ_{em} = 420–460 nm), Mito-tracker Green FM (λ_{ex} = 473 nm; λ_{em} = 490–540 nm), and CaPF-1-AM (λ_{ex} = 635 nm; λ_{em} = 655–800 nm), respectively. (d) Merged image of a, b, and c. Scale bar: 10 μm.

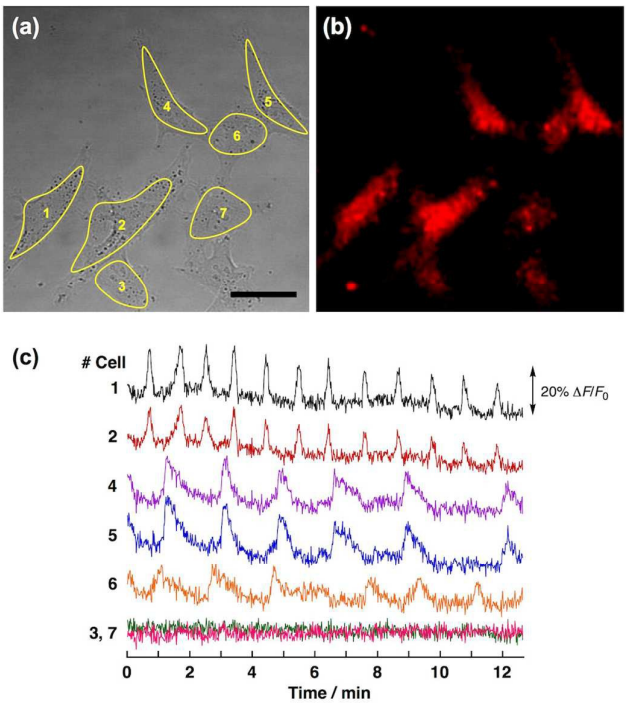

Fig. 4 Fluorescence imaging of histamine-induced Ca^{2+} oscillations in living HeLa cells with CaPF-1. Prior to the histamine stimulation, cells were stained with CaPF-1-AM (2 μM) in HBSS. Imaging was started immediately after addition of histamine to the medium with the final concentration of 1 μM. (a) Bright-field image of HeLa cells with regions of interest. The individual cells are numbered. Scale bar: 30 μm. (b) Fluorescence image of the same area in (a) observed after the stimulation with histamine. λ_{ex} = 633 nm; λ_{em} = 638–795 nm. (c) Fluorescence changes in individual cells numbered 1–7 in (a).

However, the low-lying LUMO energy level of the PF fluorophore results in a reduction potential (E_{red}) that is higher than that of fluorescein. In fact, under fully deprotonated conditions (pH = 10) in 0.1 M phosphate buffer, the E_{red} value of PF fluorophore was determined by cyclic voltammetry (–0.56 V vs. Ag/AgCl, which corresponds to –0.35 V vs. SHE) (Fig. S6, ESI†). This value is by 0.51 V higher than that of the fluorescein dianion (E_{red} = –0.86 V vs. SHE).[24] Therefore, the unfavorable Gibbs energy for the PET process in far-red dyes can be compensated, resulting in a low fluorescence quantum yield (Φ_F ~0.02) for the Ca^{2+}-free form of CaPF-1. The phosphine oxide moiety plays a crucial role for attaining high E_{red} value via effective σ^*–π^* conjugation and the inductive electron-withdrawing effect. These considerations also promise potential utility for phospha-fluorescein as a far-red-emitting fluorophore in PET-based probes that may be able to detect various other metal ions (e.g. Zn^{2+} or Hg^{2+}).

Subsequently, we examined the dependence of the fluorescence properties of CaPF-1 on the pH value. Under acidic conditions (pH = 4.8), CaPF-1 exhibited a hypsochromically shifted absorption band that was attributed to the protonated phenol form of the phospha-fluorescein (Fig. 2b). The pK_a value of CaPF-1 was determined to be 5.9 by plotting the absorbance at 636 nm against pH (Fig. S3, ESI†), revealing that the deprotonated species of PF fluorophore is dominant at cytosolic pH (7.4). This low pK_a value should be ascribed to the strong electron-withdrawing character of the phosphine oxide moiety.[20–22] However, it should be noted that the fluorescence emission of CaPF-1 at pH = 4.0 was completely quenched irrespective of the presence or absence of Ca^{2+} ions (1 mM), indicative of an efficient PET process even in the Ca^{2+}-bound form of protonated CaPF-1 (Fig. S4, ESI†).

For applications involving mammalian cells, all carboxylic acid groups in CaPF-1 have to be converted into acetoxymethyl (AM) esters (Scheme 1). We initially attempted to synthesize the AM ester of CaPF-1 by conventional methods using bromomethyl acetate, but unfortunately, only negligible amounts of the desired product were obtained. Therefore, the AM-ester of BAPTA ligand **5** was directly coupled with 4-carboxy PF **3** to afford the target in 56% yield. With this AM ester in hand, we examined the intracellular localization of CaPF-1 by co-staining with Calcein-AM, which is known to diffuse into the cytosol after hydrolysis by esterase in living cells.

HeLa cells were incubated for 30 min at 37 °C with CaPF-1-AM (2 μM) in Hank's balanced salt solution (HBSS) in the presence of 0.04% Pluronic F-127. Thereafter, the cells were washed with HBSS that contained approximately 1 mM of Ca^{2+} ions, and incubation was continued for 30 min. Then, fluorescence images were recorded using a confocal microscope (Olympus FV10i-DOC; λ_{ex} = 635 nm; diode laser). CaPF-1 showed good co-localization with Calcein, suggesting that this probe enables the detection of the concentration changes related to cytosolic Ca^{2+} signaling (Fig. S7, ESI†). Moreover, the red-shifted excitation and emission spectra of CaPF-1 allowed us to conduct multi-color staining by combination with other commercially available organelle

View Article Online
DOI: 10.1039/C7CC07344E

markers such as Hoechst 33342 and Mito-Tracker Green FM (Fig. 3).

Finally, in order to demonstrate the practical utility of CaPF-1 in intracellular Ca^{2+} imaging, the Ca^{2+} responses induced by stimulation of the histamine H1 receptor in HeLa cells was monitored.[25] After HeLa cells were stained with CaPF-1-AM (2 μM), a histamine solution in HBSS (3 μM) was added to the cell culture medium to yield the final concentration of 1 μM, and then fluorescence images were recorded every 1.04 s (Leica TCS SP8 STED; λ_{ex} = 633 nm; white light laser). As shown in Fig. 4 and the video (Movie S1, ESI†), all cells except #3 and #7 showed a time-dependent fluorescence intensity change. Because of the heterogeneous nature of receptor-mediated Ca^{2+} oscillations, each individual cell displayed different temporal dynamics as reported previously.[26] The pattern of Ca^{2+} oscillation observed in this study are in good agreement with those previously reported using various other cytosolic Ca^{2+} probes such as Fura-2,[27] Fluo-3,[27] CaTM-2,[18], and CaTM-3.[28] In their entirety, the results of this study clearly suggest that CaPF-1 is a useful tool for the detection of intracellular concentration changes of cytoplasmic Ca^{2+} ions in the far-red region.

In conclusion, we have developed a far-red emissive probe for Ca^{2+} ions based on a phospha-fluorescein scaffold. The low-lying LUMO and the narrow HOMO-LUMO gap of this fluorophore are due to an effective σ^*–π^* conjugation and the strong electron-withdrawing effect of the phosphine oxide moiety. These features should be advantageous for the development of various fluorescent probes that operate on the basis of the PET mechanism. In addition, the cytosolic-diffusible and membrane-permeable characteristics of CaPF-1 and its AM ester render this probe a promising chemical tool for monitoring Ca^{2+} dynamics in deep tissue.

This work was partly supported by JSPS KAKENHI Grant Numbers 17H05839 and JP16H06280 and JST PRESTO. ITbM is supported by the World Premier International Research Center (WPI) Initiative (Japan). MG thanks JSPS for a postdoctoral fellowship for foreign researchers.

Notes and references

1 N. Bazargani and D. Attwell, *Nat. Neurosci.*, 2016, **19**, 182–189.
2 W. Yang and R. Yuste, *Nat. Methods*, 2017, **14**, 349–359.
3 K. S. Girven and D. R. Sparta, *ACS Chem. Neurosci.*, 2017, **8**, 243–251.
4 J. Yin, Y. Hu and J. Yoon, *Chem. Soc. Rev.*, 2015, **44**, 4619–4644.
5 G. R. C. Hamilton, S. K. Sahoo, S. Kamila, N. Singh, N. Kaur, B. W. Hyland and J. F. Callan, *Chem. Soc. Rev.*, 2015, **44**, 4415–4432.
6 D. Thomas, S. C. Tovey, T. J. Collins, M. D. Bootman, M. J. Berridge and P. Lipp, *Cell Calcium*, 2000, **28**, 213–223.
7 A. Miyawaki, J. Llopis, R. Heim, J. M. McCaffery, J. A. Adams, M. Ikura and R. Y. Tsien, *Nature*, 1997, **388**, 882–887.
8 Y. Zhao, S. Araki and J. Wu, *Science*, 2011, **333**, 1888–1891.
9 M. Whitaker, *Methods Cell Biol.*, 2010, **99**, 153–182.
10 M. Kamiya and K. Johnsson, *Anal. Chem.*, 2010, **82**, 6472–6479.
11 R. Weissleder, *Nat. Biotechnol.*, 2001, **19**, 316–317.
12 S. Wäldchen, J. Lehmann, T. Klein, S. van de Linde and M. Sauer, *Sci. Rep.,* 2015, **5**, 15348.
13 E. U. Akkaya and S. Tukyilmaz, *Tetrahedron Lett.*, 1997, **38**, 4513–4516.
14 B. Ozmen and E. U. Akkaya, *Tetrahedron Lett.*, 2000, **40**, 9185–9188.
15 M. Collot, F. Ponsot and A. S. Klymchenko, *Chem. Commun*. 2017, **53**, 6117–6120.
16 T. Egawa, K. Hanaoka, Y. Koide, S. Ujita, N. Takahashi, Y. Ikegaya, N. Matsuki, T. Terai, T. Ueno, T. Komatsu and T. Nagano, *J. Am. Chem. Soc.*, 2011, **133**, 14157–14159.
17 A. Matsui, K. Umezawa, Y. Shindo, T. Fujii, D. Citterio, K. Oka and K. Suzuki, *Chem. Commun.*, 2011, **47**, 10407–10409.
18 T. Egawa, K. Hirabayashi, Y. Koide, C. Kobayashi, N. Takahashi. T. Mineno, T. Terai, T. Ueno, T. Komatsu, Y. Ikegaya, N. Matsuki, T. Nagano, K. Hanaoka, *Angew. Chem., Int. Ed.*, 2013, **52**, 3874–3877.
19 R. Y. Tsien, in *Calcium as a Cellular Regulator*, ed. E. Carafoli and C. Klee, Oxford University Press, New York, 1999, pp. 28–54.
20 A. Fukazawa, S. Suda, M. Taki, E. Yamaguchi, M. Grzybowski, Y. Sato, T. Higashiyama and S. Yamaguchi, *Chem. Commun.*, 2016, **52**, 1120–1123.
21 A. Fukazawa, J. Usuba, R. A. Alder and S. Yamaguchi, *Chem. Commun.*, 2017, **53**, 8565–8568.
22 M. Grzybowski, M. Taki and S. Yamaguchi, *Chem. -Eur. J.*, 2017, DOI: 10.1002/chem.201703456.
23 T. Myochin, K. Hanaoka, S. Iwaki, T. Ueno, T. Komatsu, T. Terai, T. Nagano and Y. Urano, *J. Am. Chem. Soc.*, 2015, **137**, 4759–4765.
24 R. G. Compton, D. Mason and P. R. Unwin, *J. Chem. Soc., Faraday Trans. 1*, 1988, **84**, 2057–2068.
25 D.-M. Zhu, E. Tekle, C. Y. Huang and P. B. Chock, *J. Biol. Chem.*, 2000, **275**, 6063–6066.
26 S. Kupzig, S. A. Walker and P. J. Cullen, *Proc. Natl. Acad. Sci. U.S.A.*, 2005, **102**, 7577–7582.
27 G. L. Ritoul and K. G. Baimbridge, *Cell Calcium,* 2003, **34**, 131–144.
28 K. Hirabayashi, K. Hanaoka, T. Egawa, C. Kobayashi, S. Takahashi, T. Komatsu, T. Uen, T. Terai, Y. Ikegaya, T. Nagano and Y. Urano, *Cell Calcium,* 2016, **60**, 256–265.

View Article Online
DOI: 10.1039/C7CC07344E

Table of contents

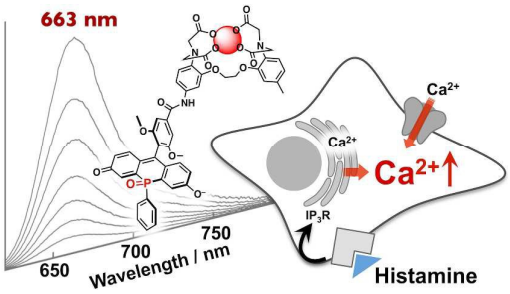

A far-red fluorescent probe based on a phospha-fluorescein scaffold enables the visualization of cytosolic Ca^{2+} dynamics in living cells.